Mesostructure of Evaporated Porphyrin Thin Films: Porphyrin Wheel Formation

Johan Hofkens, Loredana Latterini, Peter Vanoppen, Herman Faes, Karin Jeuris, Steven De Feyter, Josef Kerimo,† Paul F. Barbara,† and Frans C. De Schryver*

Department of Chemistry, Katholieke Universiteit Leuven, Celestijnenlaan 200F, 3001 Heverlee-Leuven, Belgium

Alan E. Rowan and Roeland J. M. Nolte

Department of Organic Chemistry, NSR Center, University of Nijmegen, Toernooiveld, 6525 ED Nijmegen, The Netherlands

Received: July 15, 1997; In Final Form: September 12, 1997[⊗]

The formation mechanism of ring-shaped assemblies (wheels) obtained from the evaporation of solutions of bis(21*H*,23*H*-5(4-pyrydyl)-10,15,20-tris(4-hexadecyloxyphenyl)porphyrin)platinum dichloride (PtP) has been studied by a variety of spectroscopic and microscopic techniques, including confocal fluorescence microscopy (CFM), atomic force microscopy (AFM), and near-field scanning optical microscopy (NSOM). Ring-shaped structures have been obtained by deposition of $CHCl_3$ solutions on glass, and a strong dependence of ring shape and size on the initial PtP concentration has been observed. Addition of methanol (MeOH) to the solution inhibited ring formation if the content of MeOH was higher than 10% in volume. Depositions of $CHCl_3$ solutions on graphite instead of on glass exhibited more perfect circular ring structures. Polarization and local time-resolved measurements of the fluorescence at the edge of the rings demonstrated, however, that the rings have similar spectroscopic properties on both substrates. Scanning probe microscopy techniques (AFM and NSOM) gave detailed information on the morphology of the ring. The size of the porphyrin wheels varied from 10 nm to several μm in diameter and between 10 and 200 nm in height. NSOM experiments on the nanoscale optical properties of the samples indicated that the assemblies are organized on the nanometer scale due to small molecular aggregates. Additionally, the effect of the porphyrin (PtP) concentration on the spectroscopic and scattering properties of the PtP solutions revealed that molecular aggregates are formed prior to evaporation. The implications of these results on the ring formation mechanism are discussed in this paper.

Introduction

There has been an intense interest in the spectroscopic and photochemical properties of complex molecular assemblies of photoactive molecules due to their potential application.[1−4] Furthermore ring-shaped assemblies of porphyrins are known to occur in nature, as in the bacterial complex LH2.[5]

The preparation by Schenning et al.[6] of micronscale ring-shaped assemblies of porphyrins, i.e., porphyrin rings or wheels, by evaporation of porphyrin solutions on a substrate, is one of the most interesting examples of the facile construction of molecular objects by self-assembly.

This paper reports a detailed investigation of the local optical properties of porphyrin rings on glass, obtained by deposition of porphyrin from $CHCl_3$ solutions. In particular it is concerned with the formation and characterization of porphyrin rings resulting from a detailed scanning force microscopy, near-field scanning optical microscopy,[7] and scanning confocal microscopy analysis. Using the porphyrin, bis(21*H*,23*H*-5(4-pyridyl)-10,15,20-tris(4-hexadecyloxyphenyl)porphyrin)platinum dichloride, PtP, in $CHCl_3$, thin films were grown under a variety of conditions. The ring-shaped assemblies on glass are analogous to those previously reported on a graphite surface,[6] ranging from 10 nm to 10 μm in diameter and between 10 and 200 nm in height. Emission spectra of the rings on the glass indicate that the rings are composed of porphyrin molecules in a locally aggregated configuration. Preliminary polarized NSOM images suggest that the individual aggregates in the rings are randomly oriented, leading to an amorphous conglomerate of nanometer scale aggregates. Experiments have also been undertaken to study the effect of added methanol on the ultimate film structure. The films grown on glass substrates are compared to films grown on graphite, which allows for a comparison to the previously published SEM and TEM measurements on graphite-supported films.[6] The experiments have allowed us to address some preliminary issues of the growth mechanism.

Photophysical data of the precursor in solution were studied to evaluate the role of the aggregation in the film formation.

Experimental Section

The methods for the synthesis of PtP and the film preparation techniques were presented elsewere.[6] The solvents chloroform ($CHCl_3$, Biosolve LTD, HPLC-grade), carbontetrachloride (CCl_4, Biosolve LTD, HPLC-grade), and methanol (MeOH Biosolve LTD, Spectro-grade) were used without further purification. The films investigated were stored for a few days in the dark, and no morphology changes were observed upon aging of the samples.

Spectrophotometric measurements in solution were carried out by a UV−vis spectrophotometer (Perkin-Elmer Lamda 6). Steady-state fluorescence spectra and synchronous scans were obtained by a fluorimeter (Spex Fluorolog), which provides the correction factors for the lamp profile. The fluorescence

† Permanent institution: Department of Chemistry, University of Minnesota, Minneapolis, MN 55455.

* To whom correspondence should be addressed.

[⊗] Abstract published in *Advance ACS Abstracts,* November 1, 1997.

S1089-5647(97)02305-5 CCC: $14.00

quantum yields were measured in front face configuration using cresyl violet in MeOH as a reference, $\phi_F = 0.54$.[8] In the synchronous scans, right angle configuration was used to detect the resonance light scattering from the solutions.[9] The excitation and the emission monochromators were coupled and adjusted to scan simultaneously through the range 400−800 nm. The experimental setup was tested, reproducing the data presented by Pasternack for chlorophyll *a*.[10] The scattering spectra of chlorophyll *a* in acetone in the presence of formamide-buffered solution were in agreement (within experimental error) with those reported in ref 11.

Confocal transmission images were taken with a Bischke CCD-4012P black-and-white camera. Confocal fluorescence measurements were recorded with a Biorad MRC 600 scanning unit and a Nikon Diaphot 300 inverted microscope. Fluorescence images are obtained with a 60×, 1.4 NA oil immersion objective lens (3 s/frame (768 × 512 pixels)). The frequency-doubled output (420 nm) of a Ti/Sapphire laser (Tsunami, Spectra Physics) was used for excitation. The effect of light polarization on the fluorescence has been performed by placing polarizing sheets (with parallel, perpendicular, and 45° orientations) on the excitation pulse and/or in front of the detector, respectively. Time-resolved fluorescence experiments were carried out by replacing the 460DCLP Chroma long-pass filter with a 100% reflection mirror to direct photons to a simplex MCP (Hamamatsu R3809U-50). A CVI 660 ± 5 nm narrow band-pass filter is placed in front of the MCP. As a reference 4-(dicyanomethylene)-2-methyl-6-*p*-(dimethylamino)styryl-4*H*-pyrane (DCM) in methanol, $\tau_F = 2.3$ ns,[11] has been used.

Atomic force microscopy images have been acquired in noncontact mode either by a Lumina-AFM (Topometrix) using low-resonance cantilevers and phase detection or with a Discoverer AFM system (Topometrix) using high-resonance probes and amplitude detection.

The commercial NSOM instrument (Topometrix Aurora model) was modified by replacing the 670 nm diode laser that is used for shear-force feedback with a 980 nm diode laser in order to allow for the detection of fluorescence of the porphyrin wheels (λ_{max} 665 nm, see below). Additionally, the PMT detector of the Aurora was replaced with a more sensitive and lower background level detector, namely a single-photon-counting avalanche photodiode module (EG&G, Model SPCM-200-CD1718).

Commercially available and homemade NSOM probes were employed in the experiments. The optical images were recorded with an Al-coated optical fiber probe with a nominally 100 nm aperture at the probe end; simultaneously topographic images have been recorded.

Typically 0.6 mW of 458 nm light was coupled into the fiber probe, and approximately 10^7 photons per second emanated from the probe and were detected in the far field. The excitation light was blocked by a laser notch filter (Kaiser Optical Systems, Inc. HNPF-457.9) and a 540 nm long-pass filter. Additional IR short-pass filters were employed to block the shear-force laser. The fluorescence light from the sample was collected alternatively with a 60×, 0.7 NA dry and a 100×, 1.4 NA oil immersion microscope objective. Scan speed was typically 2.2 μm/s for a 10 × 10 μm scan range, and measurements were made at room temperature.

The commercially available (Topometrix) NSOM probes were evaluated by a multistep procedure: (i) an evaluation of the mechanical response of the fiber to ensure a large-amplitude resonance with a linear motion of the probe and allowing for stable shear-force detection; (ii) an optical examination of the light emanating from the tip to ensure the absence of detectable pinholes in the aluminum coating of the probe; and (iii) a measurement of the far-field light emanating from the aperture to determine whether the intensity of the probe is sufficiently high for NSOM measurements. The resolution of the NSOM image, which is controlled by the aperture size, should be significantly better than the topographic images for tall, sharp objects (such as the porphyrin wheels). Thus, substantially better resolution in the NSOM image was used as an additional criterion for an acceptable NSOM probe.[12−14]

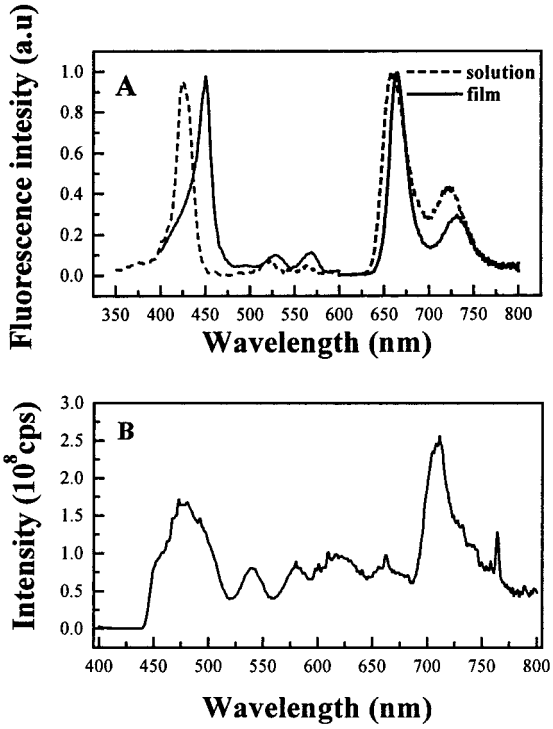

Figure 1. (A) Excitation and emission spectra of PtP deposited on glass (full line) and in $CHCl_3$ solution (dotted line); emission spectra taken on a sample prepared by evaporating a 2×10^{-4} M solution in $CHCl_3$. (B) Synchronous scan of a 5×10^{-5} M solution of PtP in $CHCl_3$.

Fluorescence spectra in the NSOM were acquired with a Chromex 250IS imaging spectrograph coupled to a cooled ICCD (Princeton Instruments, Inc. model ICCD-576-S/RB-EM). The spectra were obtained by excitation with an uncoated NSOM probe in order to increase the excitation intensity albeit with a decrease in spatial resolution.

NSOM polarization excitation measurements have been performed in collaboration with the Department of Chemistry, University of Minnesota, and the instrumental setup has been previously described.[15]

Results and Discussion

Photophysical Studies in Solution and of the Bulk Film. The spectroscopic properties of PtP in solution have been investigated in order to characterize the photophysics of the monomer building block in solution and to explore whether there is spectroscopic evidence for aggregation in the solutions that were used for film growth. Preformed aggregates may play an important role in the ring growth mechanism.

The ground state of PtP in $CHCl_3$ and CCl_4 shows an absorption spectrum typical for a metal-free porphyrin:[16] the Soret band has its maximum at 427 nm ($\epsilon = 9.0 \times 10^5$ M^{-1} cm^{-1}) and four Q-bands at 521 ($\epsilon = 3.7 \times 10^4$ M^{-1} cm^{-1})), 560 ($\epsilon = 2.6 \times 10^4$ M^{-1} cm^{-1}), 593 ($\epsilon = 1.2 \times 10^4$ M^{-1} cm^{-1})), and 650 ($\epsilon = 1.3 \times 10^4$ M^{-1} cm^{-1}) nm. The spectral shape is affected by the concentration; in particular at wavelengths below

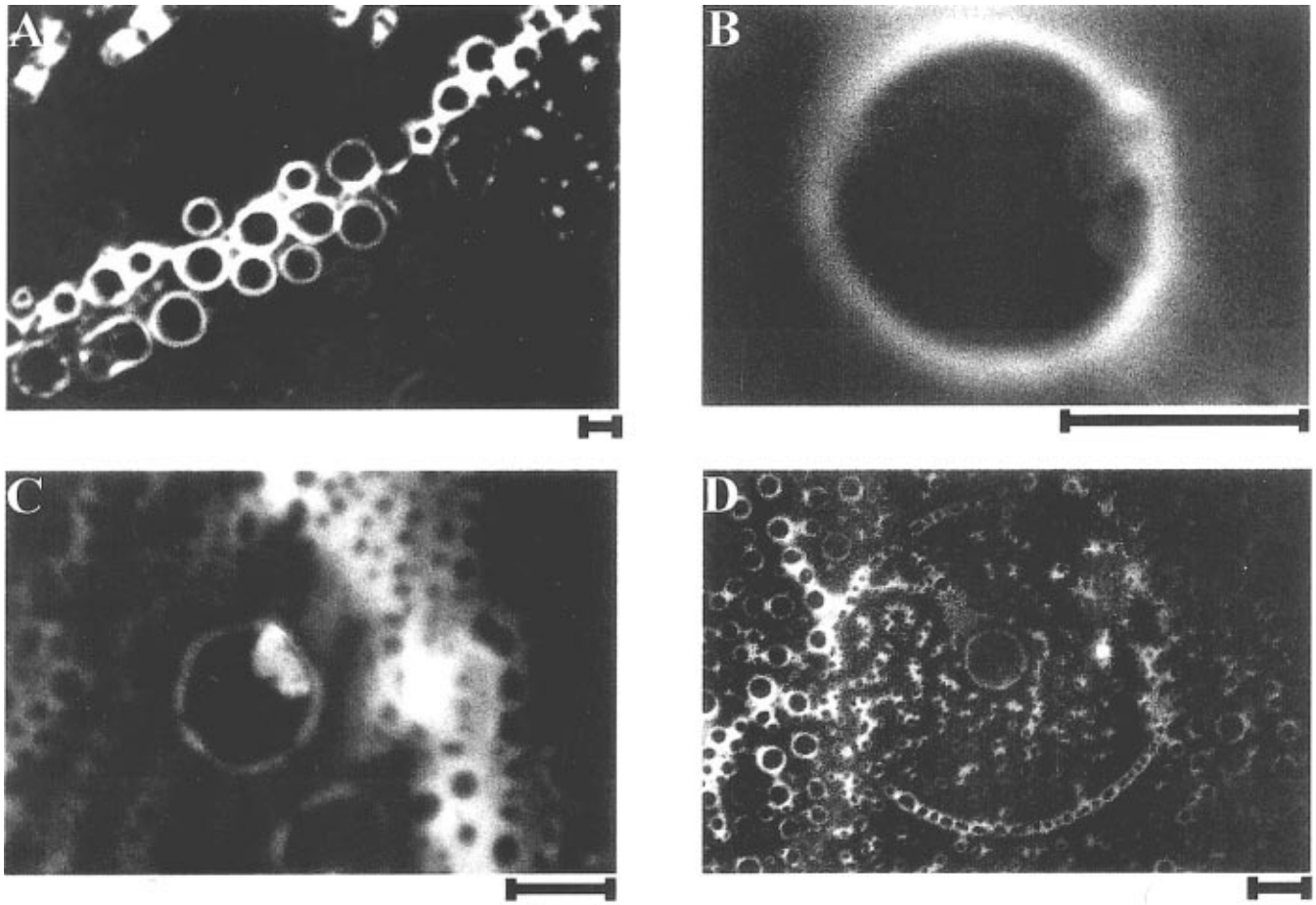

Figure 2. Confocal fluorescence images of evaporated films of PtP/$CHCl_3$ 2×10^{-6} M solutions on glass. The scale bar below each image represents 10 μm.

450 nm a deviation from the Lambert−Beer law is observed in correspondence with the broadening of the Soret band. This indicates aggregation taking place in solution. The fluorescence spectrum of PtP in $CHCl_3$ shows two bands, at 654 and 725 nm, and its shape is independent of the excitation energy. In diluted solution a fluorescence quantum yield of 0.02 has been measured. Increasing the concentration produced no additional spectral changes, but a reduction of quantum yield was observed, presumably due to aggregation. The excitation spectrum recorded at 654 nm matched the absorption spectrum (Figure 1A).

By adding MeOH to $CHCl_3$ solutions (PtP is not soluble in neat MeOH) a splitting of the Soret band is observed. In a $CHCl_3$/MeOH mixture containing 50% of alcohol, the main absorption is at 427 nm, but two new shoulders at 390 and 447 nm appear. In the presence of a higher MeOH fraction (75% in volume) the splitting is more pronounced and the absorption at 427 nm appears like a shoulder of the more intense band at 447 nm. In the presence of MeOH (50% and 75% in volume) the excitation spectrum shows a maximum at 427 nm and a shoulder at 445 nm, so it does not match the absorption spectrum. These effects are probably induced by the stacking among the PtP dimers, which alters the local transition dipoles. One possible explanation is the formation of a sandwich-like complex in which the porphyrin aromatic rings stack together.[17]

As it has been shown by Pasternack et al.,[11,12,18] light scattering at wavelengths in the absorption band envelope (a form of resonance light scattering) of an aggregate in solution can be considerable if the absorption is not too strong and the particle size is sufficiently large and can be used as an indication of aggregation. Synchronous fluorescence scans have been

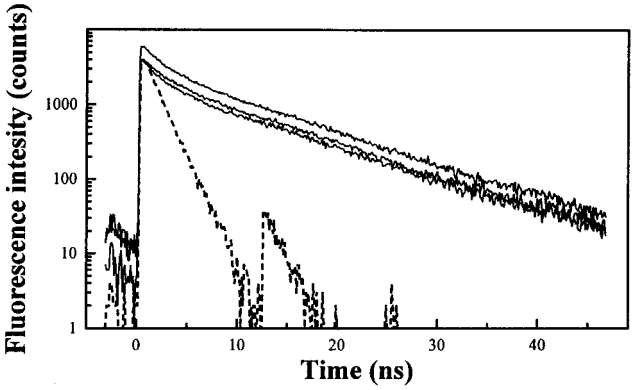

Figure 3. Decay curves obtained by scanning the amorphous material between rings (full line), an isolated ring (bold line), and an aggregate in a ring (thin line). The dotted line is the decay of the reference.

carried out on PtP in $CHCl_3$ solutions at different concentrations. When the concentration is higher than 10^{-5} M, resonance light scattering could be detected, and its intensity increases with the concentration. In particular, Figure 1B shows that throughout the range 400−600 nm the scattering was weak ($\sim 10^7$ cps) due to the big absorption of PtP, as demonstrated by the decrease of scattering at the position of the Soret band. However, a higher scattering intensity was observed at longer wavelengths, with a maximum at 710 nm. This result indicates the presence of aggregates also in $CHCl_3$, but the absence of remarkable changes in the absorption and excitation spectra suggests that they are not stacked.

The spectroscopy of PtP in solid thin films has also been investigated. The ground-state absorption of the bulk film is

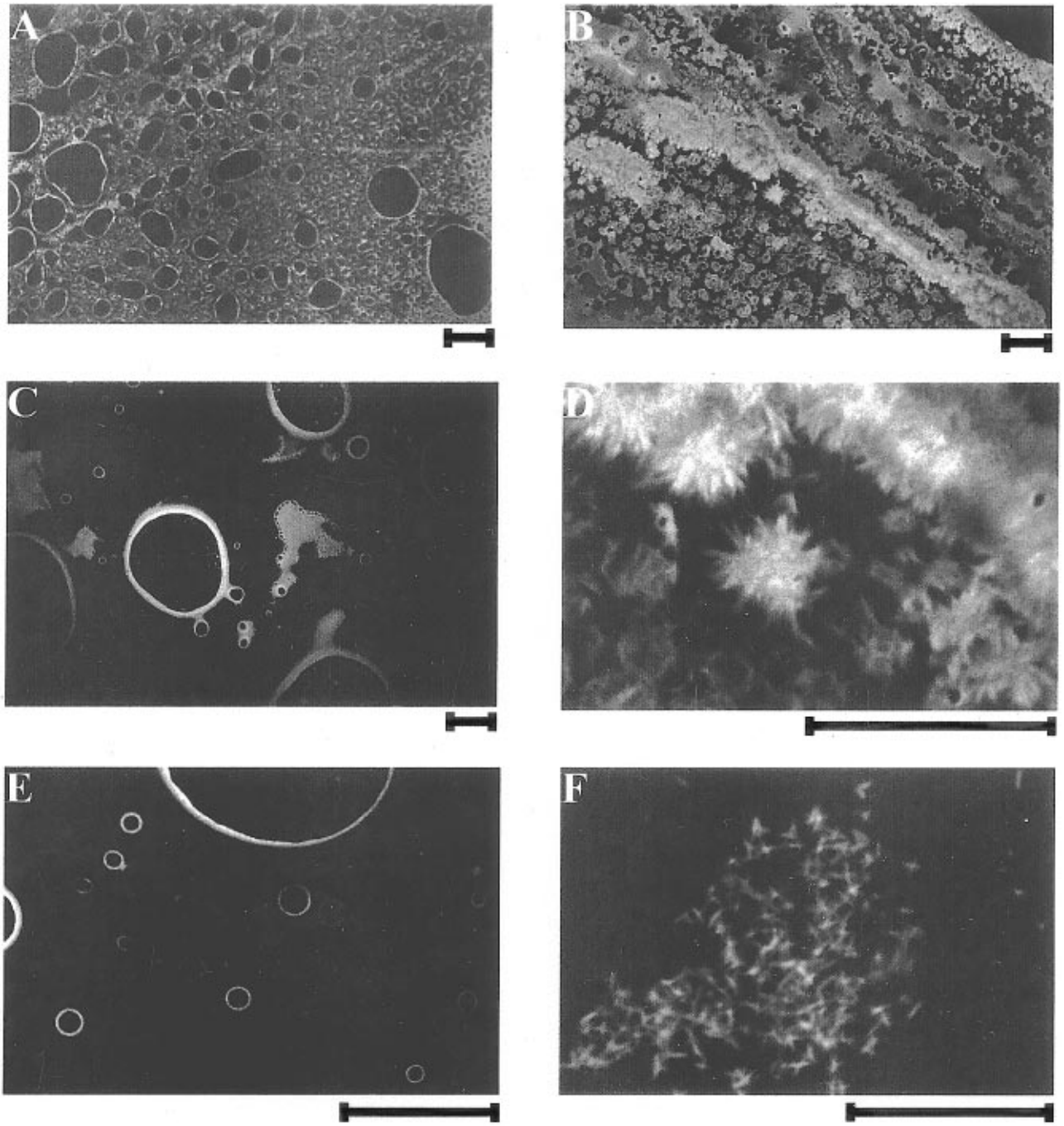

Figure 4. Confocal fluorescence images of evaporated films of PtP in mixtures of $CHCl_3$ and MeOH. (A, C, E) Images taken at different positions of a sample prepared from a solution with 3% of MeOH. (B, D) Images recorded from a sample prepared by a solution with 6% of MeOH. (F) Image obtained from a sample prepared by deposition of a solution containing 28% of MeOH. The scale bar below each image represents 20 μm.

red-shifted compared to the one measured in solution. The changes are more pronounced for the Soret band region, which has its maximum at 450 nm. The fluorescence spectrum of PtP on glass has a main band at 665 nm and a second one at 735 nm. The excitation spectrum recorded at 665 nm matches the absorption spectrum. Figure 1A shows the normalized excitation and emission spectra of the bulk film and the solution for comparison. The spectral properties of these films were the same, irrespective of the concentration of the starting solution.

Confocal Fluorescence Microscopy of the Porphyrin Thin Films. We used CFM to study a broad range of porphyrin thin films, including samples prepared from PtP dissolved in mixtures of $CHCl_3$/MeOH with various compositions. Time-resolved fluorescence measurements were combined with confocal measurements to monitor the time-resolved emission dynamics of porphyrin rings. Porphyrin rings on graphite substrates were also examined.

Confocal images in transmission and fluorescence mode showed that the morphology of the structures was affected by the concentration of the starting solution. By varying the concentration of the solution, different structures have been grown that range from rings that are highly interrupted (like beads on a chain) to thick, well-formed rings. For very highly concentrated starting solutions, a continuous deposition of material has been observed in the films (see below for details). The films obtained from 2×10^{-6} M PtP solution exhibit especially well-formed rings which gave the best resolved images with CFM, in terms of contrast and background fluorescence.

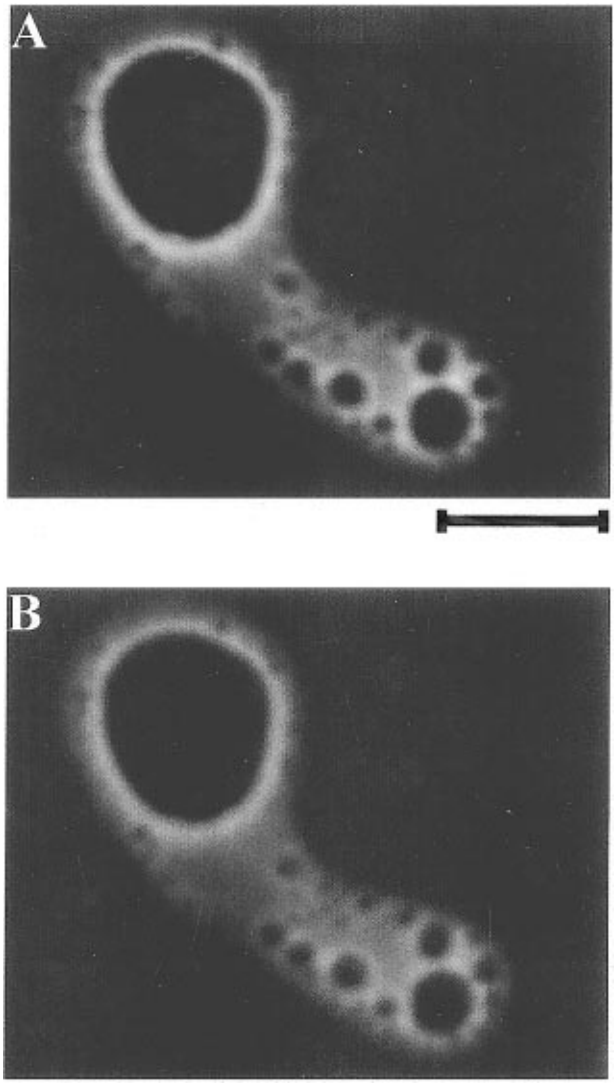

Figure 5. Confocal fluorescence polarization images of evaporated films of PtP in a mixture of $CHCl_3$ and 3% MeOH on glass. The scale bar below each image represents 10 μm.

Figure 2 portrays CFM images of a porphyrin thin film sample on glass prepared by evaporation of a 2×10^{-6} M PtP solution. These data show some isolated rings and other regions with fused rings and some even more complex structures, such as the complex of rings shown in Figure 2D. It is likely that these various assemblies result from an organization that occurs in the growth mechanism. Thus, the ring of rings is an extreme example of the organizing structures fusing together, which is apparent in Figure 2A. Some of the rings have a large individual deposition on one side which may function as a nucleation site (Figure 2C). With CFM no fluorescence has been detected from the inside of the rings.

An example of time-resolved fluorescence decays for the porphyrin rings is shown in Figure 3. The decay kinetics of different regions of the sample are, within experimental error, indistinguishable. The three traces in Figure 3 correspond to the isolated ring in Figure 2B, the region of the sample that includes many fused rings (Figure 2C), and finally the large bright region of material attached to the ring in Figure 2C, respectively. The similarity of these decays reveals that the porphyrin material that comprises the rings, the large composite aggregates, and the material between the rings presents a very similar structure at the spatial resolution of CFM.

An examination of the images of films grown in different conditions showed a variety of features that were consistent with

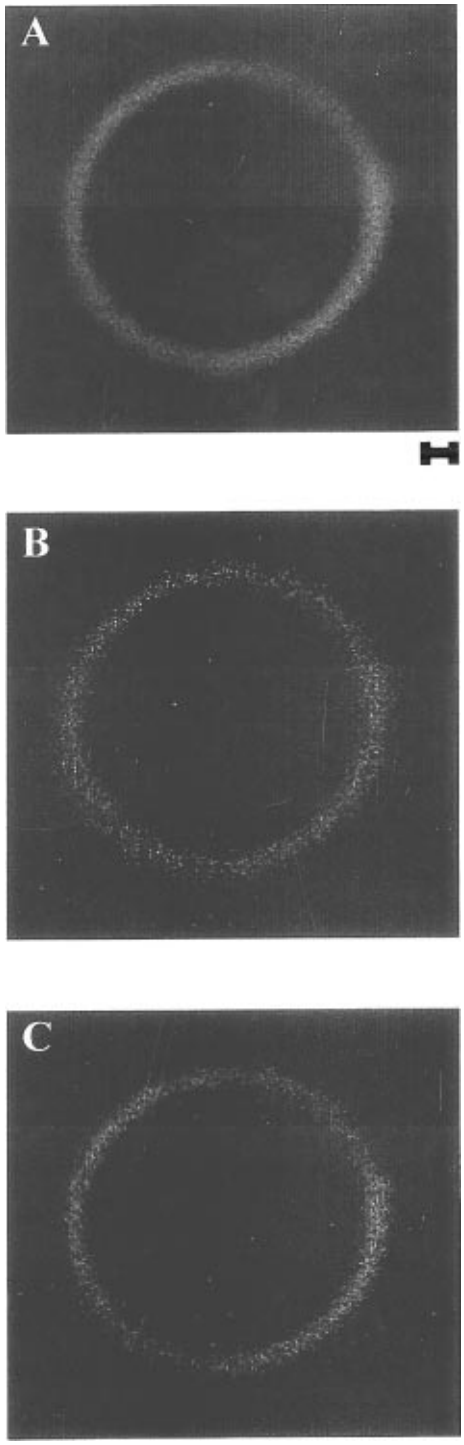

Figure 6. Confocal fluorescence polarization images of evaporated films of PtP/$CHCl_3$ on graphite, using (A) unpolarized light and (B) horizontally and (C) vertically polarized light. The scale bar below each image represents 1 μm.

two possible mechanisms for porphyrin ring formation. In a first model, the aggregation is induced by the gas bubbles formed during the evaporation of the porphyrin/$CHCl_3$ solutions that are used to prepare the films (bubble model). At the circumference of the bubble, nucleation and growth of a porphyrin amorphous phase should occur, which results in ring structures after the evaporation was complete. In general, bubble-induced aggregation is a well-documented phenomenon.[19] In a second model, the assembly of porphyrin material can be induced by a dynamic process during the dewetting of the substrate by the $CHCl_3$ solutions. The unstable film evolves via nucleation and growth of dry patches (hole model).[20] The

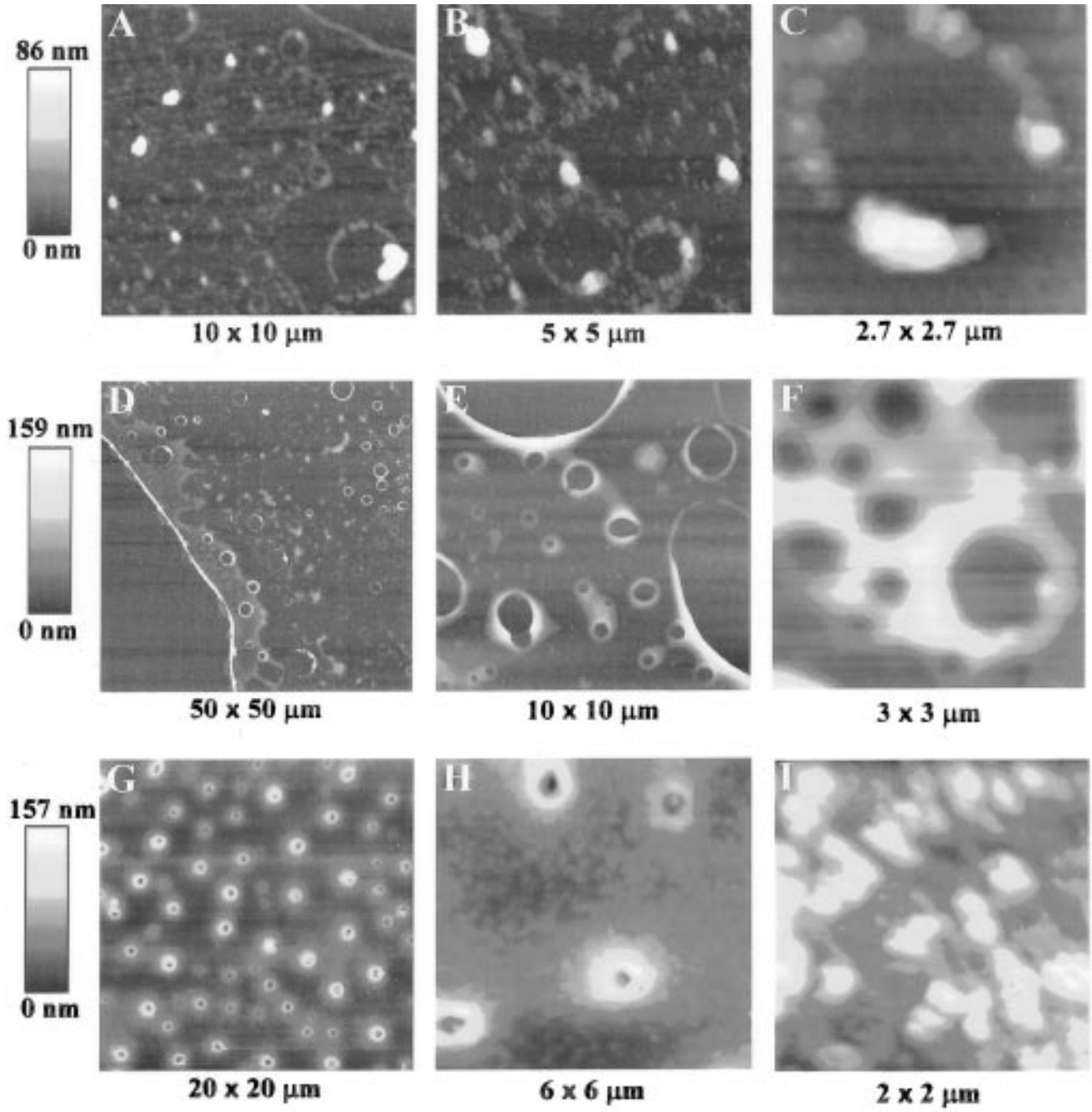

Figure 7. Topographic images of evaporated films of PtP/$CHCl_3$ solutions on glass microscope cover slips. Image size is indicated below each image. (A−C) Images taken from a sample prepared by solvent casting of a 2×10^{-7} M solution. Images A and B are acquired by noncontact AFM while image C was acquired by shear-force with a coated NSOM probe. The color scale on the top left applies for image A. Images B and C have similar color scales. (D−F) Images scanned by noncontact AFM on a sample prepared by solvent casting a 2×10^{-6} M solution. The color scale on the middle left applies for image D; images E and F have similar color scales. (G−I) Images taken by shear-force with an uncoated NSOM probe on a sample prepared by spin coating a 2×10^{-4} M solution. The bottom left color scale corresponds to the height contrast in image G and is appropriate for image H. Image I is a close up of an area between the rings shown in images G and H. The contrast in Figure 1 corresponds to about 30 nm.

hole expands (due to capillary forces) and induces the displacement of the porphyrin material and its accumulation at the hole rim. This ends in ring structures when the drying is complete. The self-assembly of material, induced by a dry hole nucleated during wetting and dewetting processes, has also recently been reported.[21] The process is a complex phenomenon which requires an organizing structure (bubble/hole), and it involves hydrodynamic and surface effects. It will be discussed elsewhere in detail.

Samples were also prepared from the PtP solutions using $CHCl_3$/MeOH mixtures as the solvent. The film morphology is altered by the presence of MeOH, as demonstrated in Figure 4. In the films with only 3% MeOH, ringlike structures are observed. At the edge of the film, where the porphyrin concentration is particularly high, many ring structures are observed with a large distribution of ring diameters (Figure 4A). Many of the rings are fused together, and the larger rings are significantly distorted from the circular shape. Near the center of the same film, the ring density is much lower and individual rings are easily observed (Figures 4C,E).

Further addition of MeOH to the PtP solution significantly suppresses ring formation. For 6% MeOH solutions, few rings are observed, but structures of micrometer size conglomerate of aggregates are observed, especially at the edge of the film;

see Figures 4B,D. Finally, at high MeOH concentration, e.g. 28%, the CFM images reveal a high degree of micrometer size depositions surrounded by regions of no fluorescence, which is portrayed in Figure 4F.

These results suggest that wetting and dewetting of the substrate may play an important role in the deposition process. Two possible explanations for the suppression of ring growth by adding MeOH can be suggested. First of all, the wetting of the glass substrate by the solution should be enhanced in the presence of MeOH due to its more polar and hydrogen-bonding character than $CHCl_3$ (the initial size of the solution droplet is observed by eye to be significantly larger for the solutions with higher MeOH content). The improvement of wetting alters the thermodynamics of the liquid layer on the substrate and may change the rate of bubble nucleation and/or bubble attachment to the surface. Furthermore, MeOH appears to alter the molecular packing of the porphyrins in the aggregate, and this may in turn favor the formation of fiberlike assemblies of aggregates.

Figure 5 compares polarized fluorescence CFM images of porphyrin rings prepared from $CHCl_3$/MeOH solution. The horizontally and vertically polarized fluorescence images are identical within experimental error. Similar images have been obtained when the polarization of the excitation light is changed. The absence of fluorescence anisotropy in the CFM images indicates that no ordered structures could be observed within the spatial resolution (ca. 400 nm scale) and the instrumental sensitivity.

Preliminary CFM measurements have also been made for porphyrin rings grown by evaporation of PtP/$CHCl_3$ solutions on a graphite-coated copper grid. The results are highly consistent with TEM images of analogous samples.[6] Unpolarized (Figure 6A) and horizontally and vertically polarized images (Figures 6B,C) demonstrate that the fluorescence properties from the porphyrin rings on graphite surfaces are analogous to those on glass surfaces. But on graphite the structures appear more perfectly circular-shaped and most of the fluorescent material is assembled in the rings and not at the outside.

Scanning Probe Measurements. Using scanning probe microscopy, a deeper insight into the morphology of solvent-evaporated porphyrin thin films has been reached. Two types of scanning force images have been considered, namely noncontact AFM and shear-force microscopy measurements.

Figure 7 portrays various scanning force images of thin films prepared from the deposition of PtP in $CHCl_3$ solutions on glass substrates. Images A−C correspond to 2×10^{-7} M PtP solution, while D−F correspond to a 2×10^{-6} M solution, and G−I correspond to 2×10^{-4} M. The well-formed rings, obtained from the 2×10^{-6} M solution, vary in height from 10 to 200 nm and in diameter from 10 nm to 10 μm. Images 7A−C exhibit ring-shaped assemblies that are built up from individual isolated particles like beads on a necklace. Almost every ring has exactly one larger particle on its edge. The rings are somewhat smaller in diameter than those prepared from higher concentration solutions. The heights of the beads that comprise most of the rings are substantially less than the heights of the well-formed rings prepared from high-concentration solutions. Noncontact AFM (Figure 7A,B) and shear-force microscopy (Figure 7C) exhibit very similar topographic images, as expected for artifact-free imaging (in contrast to the situation for the films grown from more concentrated solutions; see below).

A line scan analysis of the AFM image Figure 7A is shown in Figure 8A for a line drawn through the edges of one of the larger rings. Note that the level of the material between the rings and between the beads on the rings is at the level of the glass substrate and that the individual beads are on the order of tens of nanometers for the smaller beads. In Figures 9A,B a pair of simultaneous topographic and fluorescence NSOM images are shown for an identical region of 2×10^{-7} M sample. These data confirmed that each of the beads, including the single very large bead that comprises each ring, is comprised of porphyrin material. This is particularly obvious in Figure 9C, which is a close-up of the middle right ring in Figure 9B.

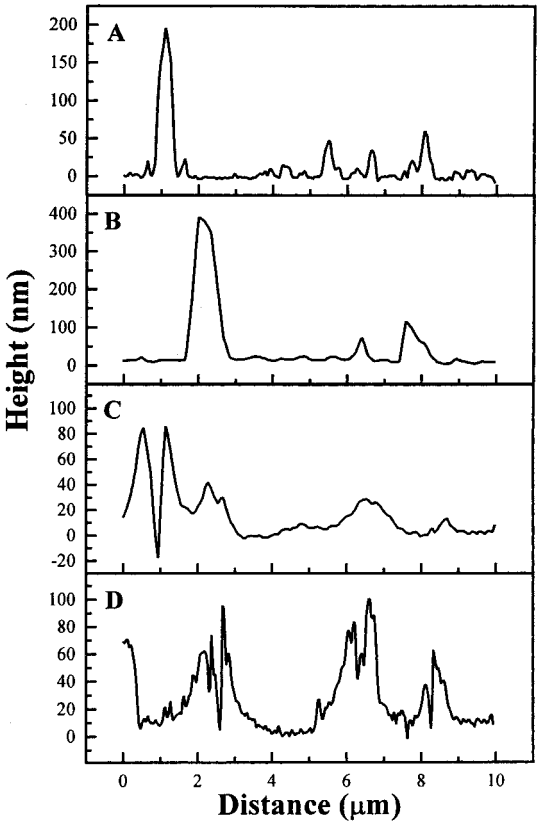

Figure 8. Selected line scans in the topographic images shown in Figure 7. (A) Topographic line scan in Figure 7A. (B, C) Topographic line scans from a 10×10 μm cutout of respectively part D and G of Figure 7. (D) Topographic line scan from an image (not presented) taken with shear-force with a coated NSOM probe on a sample prepared by spin coating a 2×10^{-4} M solution.

The scanning probe measurements on the 2×10^{-7} M film are easily interpreted in terms of the bubble- or hole-induced ring growth mechanisms. Each ring in the image corresponds to an individual bubble during the evaporation or to a hole formed in the dewetting process. The presence of one large bead or aggregate on each ring suggests that this may be the nucleation site for the deposition. The incomplete ring structure and the relatively small ring height observed for the films grown from 2×10^{-7} M solutions are probably a result of the limited amount of PtP that is available at this concentration during ring growth.

These interpretations apply equally well to the films grown from the 2×10^{-6} M PtP solutions, for which AFM images are shown in Figure 7D−F. Simultaneous shear-force and fluorescence NSOM images are shown in Figure 9D−F, respectively. Parts D and E are simultaneously acquired topographic and fluorescence images; F is a close-up of the upper right ring of the previous figures. The individual rings are generally closed and higher than the rings from 2×10^{-7} M solutions; in some cases they are fused together. A line scan (Figure 8B) of the AFM topographic image reveals that the height of the sample inside the rings is at the level of the glass substrate. Additionally, regions of the sample outside the rings

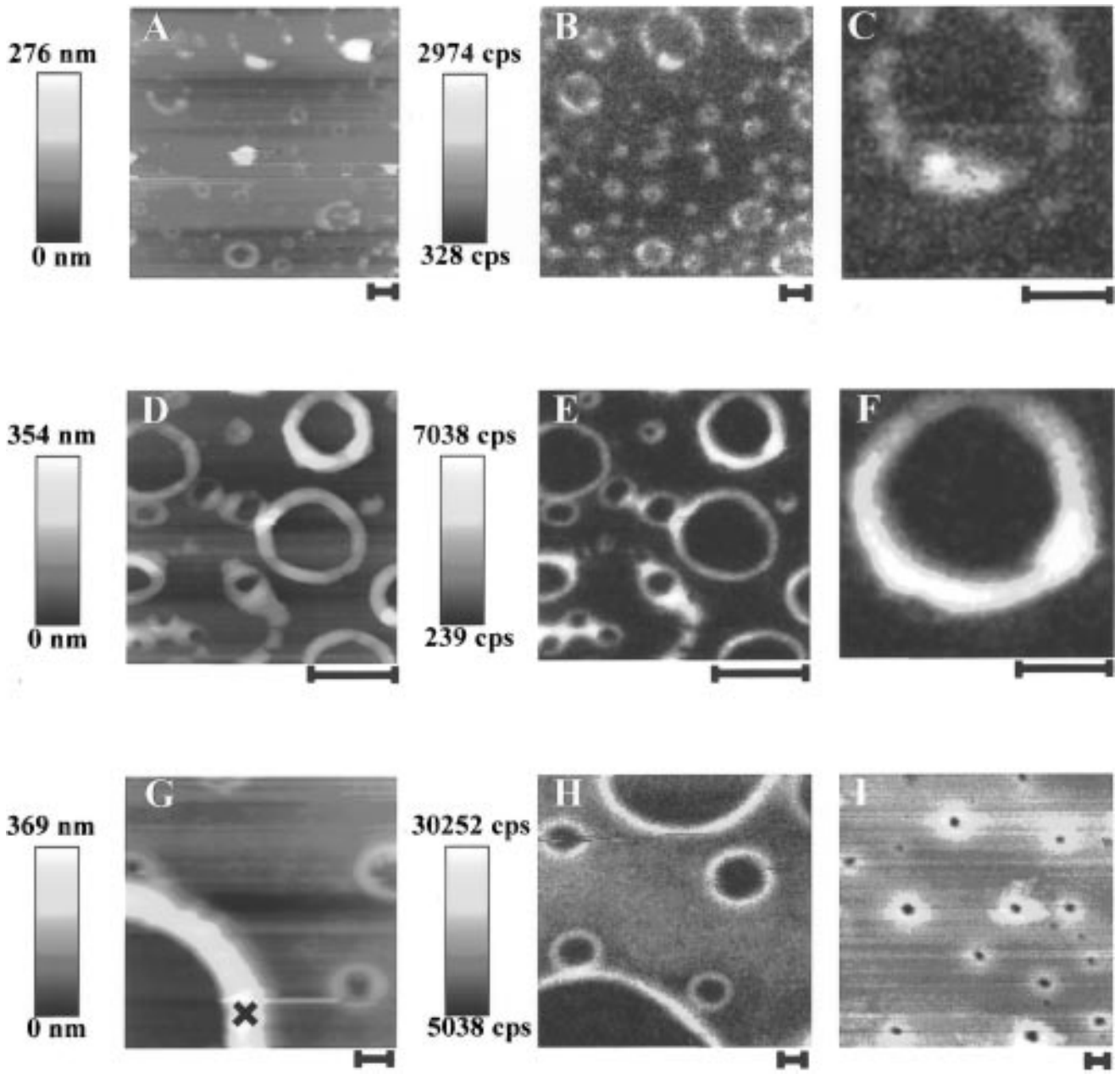

Figure 9. Near-field and topographic images of evaporated films of PtP/$CHCl_3$ solutions on glass. The black scale bar below each image represents 1 μm. (A, B) Topographic and corresponding near-field image taken on a sample prepared by solvent casting of a 2×10^{-7} M solution. (C) Enlarged view of the top middle ring displayed in B. (D, E) Topographic and corresponding near-field image taken on a sample prepared by solvent casting of a 2×10^{-6} M PtP/$CHCl_3$ solution. (F) Enlarged view of the top right ring displayed in B. (G, H, I) Topographic and near-field images taken on a sample prepared by solvent casting of a 1×10^{-4} M PtP/$CHCl_3$ solution. H is taken in the middle of the droplet, while I is taken at the edge of the sample. The $\times$ in G indicates the position where spectra were acquired. The color scale beside figure H only applies for I. For I the color scale beside E is valid.

are either at the level of the glass substrate or at a higher level if the excess material between the rings is present at that region of the sample.

The topography and NSOM images are highly correlated, suggesting that the NSOM data are primarily a measure of the amount of porphyrin material present. Note that the shear-force image recorded with coated NSOM tips exhibits lower resolution (broader rings) than the fluorescence NSOM. This is a result of the relatively poor topographic resolution in the sample plane of the Al-coated NSOM probe. The fluorescence NSOM image has significantly better spatial resolution since it is limited by the optical aperture size of the probe.

The presence of well-formed rings for the 2×10^{-6} M solution indicates that in these higher concentration solutions there is sufficient material for completion of the ring structure during the deposition process. The excess material is probably due to further deposition of aggregates after ring growth is complete. The apparent absence of a single large nucleation site on each ring is in contrast to that described above for the 2×10^{-7} M films. This may reflect a different rate of nucleation for the higher concentration solutions, but alternatively may be a consequence of the large amounts of material present in the 2×10^{-6} M rings which may include (and hide) the original nucleating porphyrin aggregate.

Even more excess material between the rings is observed for solutions deposited from a 2×10^{-4} M PtP solution. The films represent a continuous structure with pinholes which correspond to small porphyrin rings. The porphyrin rings take on the shape of volcanolike assemblies that protrude above the continuous film; see Figures 7G,H and 8C,D. Figure 9G−I represents

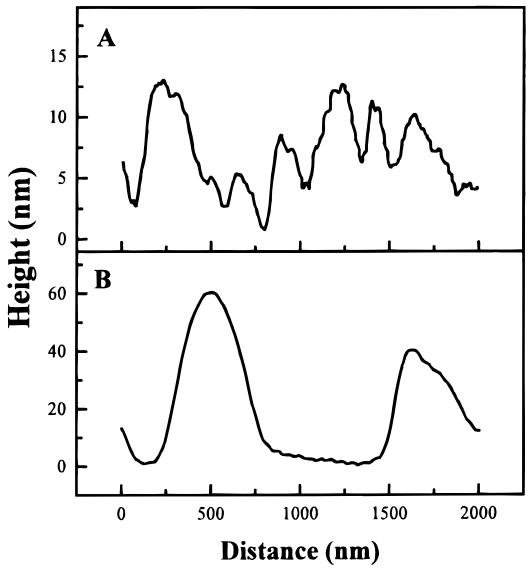

Figure 10. Selected topographic line scans on a 2 μm length scale. (A, B) Line scans taken from parts F and I of Figure 7, respectively.

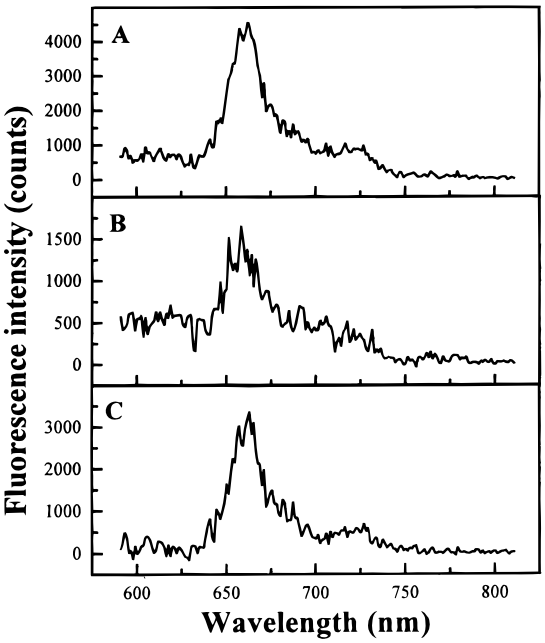

Figure 11. (A) Spectrum taken on the rim of the ring shown in Figure 7C. Acquisition time 60 s. (B) Fourth spectrum in a row with acquisition time of 60 s on the same position. (C) Difference spectrum of A and B.

topographic and fluorescence images taken in different regions of the sample. Figure 9H is a fluorescence image taken at the center of the droplet, where still well-formed rings are present. While the fluorescence intensity in the rings is at the background level, the intensity between rings is distinctly higher. This can be explained by the presence of excess material between rings. At the edge of the droplet, the small pinholelike structures that were observed in AFM are also observed in the fluorescence image (Figure 9I). A possible explanation for the smaller structure size, observed in both AFM and fluorescence, can be related to the solution density, which should increase with the PtP concentration. This should affect the solution vapor pressure and ultimately its evaporation rate and also the dynamics of the liquid film on the glass.

Considering the complex structure of these films, which involves organization on length scales ranging from the molecular to nearly the macroscopic, it is challenging to define the structure and organization of these films in well-defined terms. Thus terms such as aggregate size, film morphology, and surface smoothness are qualitative at best for these complex materials. Nevertheless, we have attempted to determine a typical aggregate size for the various films by using scanning force microscopy on a small scale (Figure 7F,I). For this analysis, we emphasize the more concentrated films and in particular the regions of these films where continuous porphyrin material is present. For example, for the 2×10^{-6} M films, there is little evidence of aggregate structures that can be resolved by noncontact AFM or shear-force measurements. In other words, on the nanometer scale, except for the ring structures, the films appear continuous with a smooth profile, especially in the regions of excess material between the rings. In particular, the images do not exhibit the typical features of resolvable individual crystalline regions such as sharp edges and angular intersections. Line scans of these results are shown in Figure 10. For the 2×10^{-6} M films, noncontact AFM (Figure 10B) reveals a surprisingly smooth profile for the continuous material nearby the rings. The data, therefore, indicate that the actual size of an individual aggregate must be less than the spatial resolution of these techniques, i.e., <25 nm. The apparently larger aggregates that are clearly observed in the 2×10^{-4} M film (see Figure 10A) are probably themselves assembled from much smaller aggregates.

Attempts have also been made to study the aggregate size of the continuous material that is present between the rings of the highly concentrated 2×10^{-4} M films. Noncontact AFM imaging of these films was not successful due to unstable feedback of the tip sample separation that apparently resulted from continuous alteration of the sample surface by interaction with the AFM probe. This seems to indicate that the sample surface is fragile, perhaps involving a low-density composite of weakly bound aggregates. Shear-force imaging in these regions, in contrast, was accomplished with stable shear-force feedback, consistent with the relatively weak sample force interaction for shear-force measurements. The shear-force topographic images recorded in the continuous region between the volcanoes exhibited a surface roughness of approximately 10 nm due to structures with apparent widths of 50−100 nm, as shown in Figures 7I and 10A. It is unknown whether these structures are related to the aggregate composites that are observed in the films grown from the lower concentration PtP solutions. The apparent contradiction between the relatively smooth profiles seen by noncontact AFM for the 2×10^{-6} M films and the relatively rough surfaces seen for the 2×10^{-4} M films may be a further reflection of the complex morphology of thin films that are prepared from complex self-assembly mechanisms. The rough surface can be due to deposition of larger structures built up from smaller aggregates. Unfortunately, the surface profile measurements, especially for the nanometer scale, may be partly affected by artifacts due to the fragile nature of these films.

Emission spectra taken at the cross in Figure 9G of the film have been recorded with excitation from an uncoated NSOM probe (excitation spot size approximately 500 nm). Figure 11A,B shows spectra recorded for a period of 60 s each during irradiation on the edge of the porphyrin ring shown in Figure 7C. Figure 11A corresponds to the 60 s immediately after irradiation was initiated, while Figure 11B was recorded after irradiation was in progress for a period of about 200 s. These data and other spectra recorded during the intervening period (not shown) exhibit a decrease in the intensity of the porphyrin

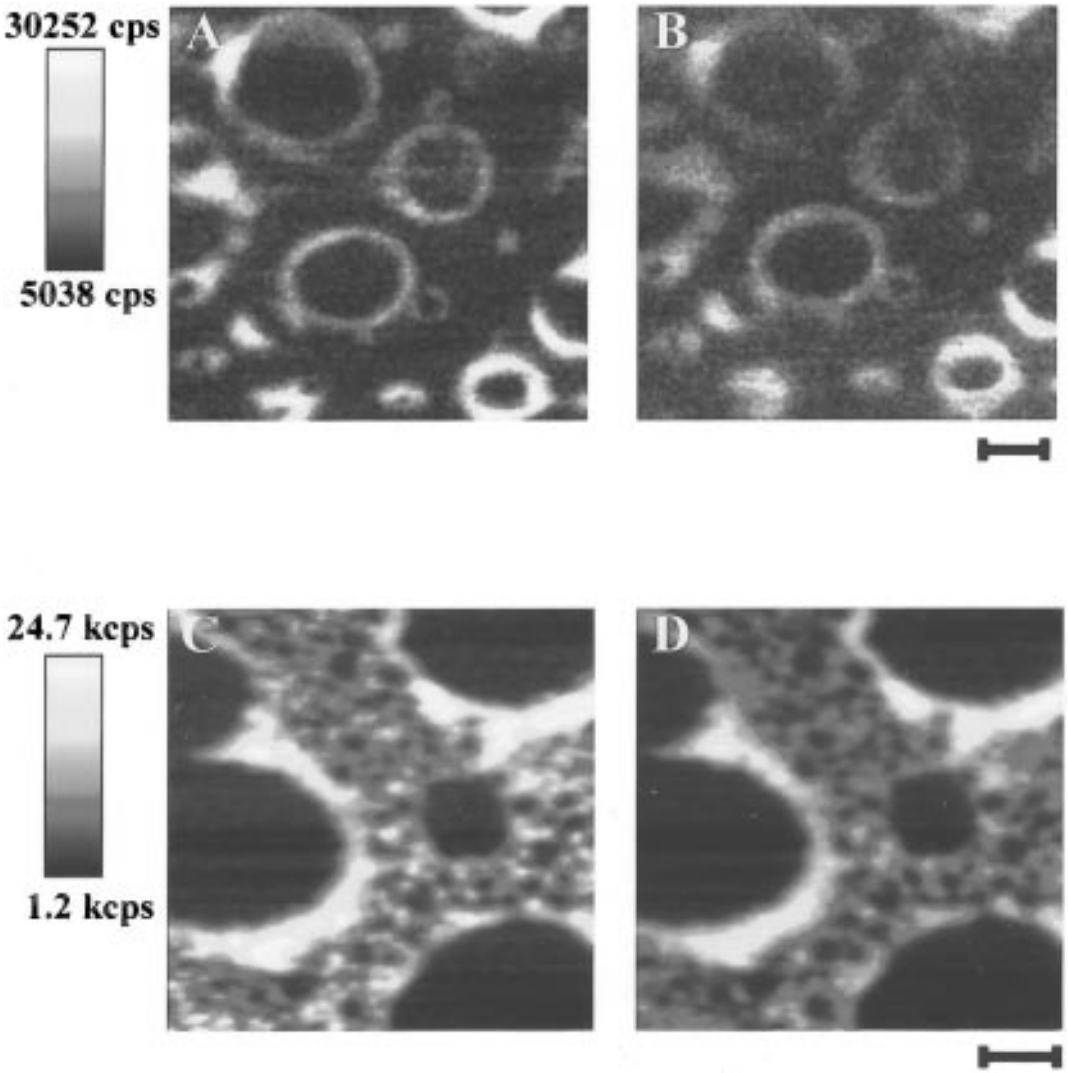

Figure 12. NSOM polarized emission fluorescence images recorded on a sample prepared from a 2×10^{-6} M solution. Nonpolarized excitation light was used in A and B, while in C and D linearly polarized light was used to excite the sample. (C) Emission detected in parallel polarization with respect to the excitation. (D) Emission detected in perpendicular polarization with respect to the excitation. The scale bar below each image represents 1 μm.

emission with time due to photobleaching of the irradiated region of the ring. It should be noted that the intensity scale in Figure 11B is much smaller than that for Figure 11A. The broad background emission that is especially apparent in Figure 11B (for example at 600 nm) is essentially due to fluorescence from the uncoated fiber probe, not to the sample. The background emission has been removed from the data by subtracting Figure 11B from Figure 11A, resulting in the corrected emission spectrum that is shown in Figure 11C. At the position of the continuous film the spectrum is similar. In particular no spectral shifts have been observed.

Parts A and B of Figure 12 are fluorescence polarization images acquired using nonpolarized excitation light. Although the intensity scale of both images is different, the fluorescence distribution is similar in the two images. On the other hand, when linearly polarized excitation light is used, different intensity distributions have been observed. Figure 12C,D shows preliminary NSOM polarized excitation measurements. The photoselection of small aggregates (on the order of 10^2 nm) is observed in the fluorescence images which were recorded by the detection of the emitted light with parallel and perpendicular polarization with respect to the excitation. This indicates the presence of order on the nanometer scale.

Conclusions

Scanning confocal microscopy and scanning probe microscopies have been used to characterize the morphology and molecular organization of thin films grown by evaporation of solutions of the porphyrin PtP. Several features in the images lead to new insights on the growth mechanism of porphyrin rings. For deposition of solutions of optimal PtP concentrations, ring-shaped assemblies of PtP were clearly observed in the films. For low PtP concentration, however, only partially formed rings were present, and for extremely high PtP concentrations the ring-shaped assemblies are surrounded by excess PtP material. Preliminary polarized NSOM images showed the presence of ordered structures on the nanometer scale upon photoselection of small aggregates. The individual aggregates, however, are randomly oriented, indicating that the rings are an amorphous conglomerate of aggregates. Several features in the images lead to new insights on the growth mechanism of porphyrin rings. Separate spectroscopic measurements on the PtP solutions used for ring preparation lead to several indications that these solutions contain nanometer scale porphyrin aggregates.

The data are discussed in terms of two possible mechanisms involved in the ring formation: a model that is based on induced bubble aggregation and a model based on hole-assisted assembly

during the dewetting phenomenon. The results indicate that the nucleation structures probably result from preformed porphyrin aggregates.

Acknowledgment. We thank Dr. R. Blossey, Dr. M. Voué, and Prof. J. De Coninck for interesting and stimulating discussions. J.H. and L.L. thank FWO for postdoctoral fellowships as S.D.F. for a predoctoral fellowship. This work was supported by FWO and DWTC through IUAP-4-11 and by the Dutch Foundation for Chemical Research (SON) with financial aid from the Dutch Foundation for Chemical Research (NWO). P.F.B. was supported by a fellowship from KU Leuven.

References and Notes

(1) Guengerrich, F. P. *J. Biol. Chem.* **1991**, 266, 10019.
(2) Zuber, H.; Brunisholz, R. A. In *Chlorophylls*; Scheer, H., Ed.; CRC Press: Florida 1991; p 627.
(3) van Esch, J.; Roks, M. F.; Nolte, R. J. M. *J. Am. Chem. Soc.* **1986**, *108*, 6093.
(4) Schenning, A. P. H. J.; Hubert, D. H. W.; Feiters, M. C.; Nolte, R. J. M. *Angew. Chem., Int. Ed. Engl.* **1994**, *23/24*, 2468.
(5) Kühlbrandt, W. *Nature* **1995**, *374*, 497.
(6) Schenning, A. P. H. J.; Benneker, F. B. G.; Guerts, H. P. M.; Liu, X. Y.; Nolte, R. J. M. *J. Am. Chem. Soc.* **1996**, *118*, 8549.
(7) Betzig, E.; Trautman, J. K. *Science* **1992**, *257*, 189.
(8) Scaiano, J. C. *CRC Handbook of Organic Photochemistry*; CRC Press: Boca Raton, FL, 1989.
(9) Pasternack, R. F.; Bustamante, C.; Collings, P. J.; Giannetto, A.; Gibbs, E. J. *J. Am. Chem. Soc.* **1993**, *115*, 5393.
(10) de Paula, J. C.; Robblee, J. H.; Pasternack, R. F. *Biophys. J.* **1995**, *68*, 335.
(11) Hofkens, *J.* Ph.D. Thesis, K.U. Leuven, 1993.
(12) Xie, X. S. *Acc. Chem. Res.* **1996**, *29*, 598.
(13) Heinzelmann, H.; Huser, T.; Güntherodt, H.-J.; Pohl, D.; Hecht, B.; Novotny, L.; Martin, O. J. F.; Hafner, C. V.; Baggenstos, H.; Wild, U. P.; Renn, A. *Opt. Eng.* **1995**, *3*, 2441.
(14) Vanden Bout, D. A.; Kerimo, J.; Higgins, D. A.; Barbara, P. F. *Acc. Chem. Res.* **1997**, *30*, 204.
(15) Higgins, D. A.; Kerimo, J.; Vanden Bout, D. A.; Barbara, P. F. *J. Am. Chem. Soc.* **1996**, *118*, 4049.
(16) Gouterman, M. In *The Porphyrins*; Academic Press, Inc.: New York, 1978; Vol. III A, Chapter 1.
(17) Kasha, M. *Radiat. Res.* **1963**, *20*, 55. Eriksson, S.; Källebrin, B.; Larsson, S.; Matensson, J.; Wennerström, O. *Chem. Phys.* **1990**, *146*, 165.
(18) Pasternack, R. F.; Shaefer, K. F.; Hambright, P. *Inorg. Chem.* **1994**, *33*, 2062.
(19) Judd, R. L.; Lavdas, C. H. *J. Heat Transfer* **1980**, *102*, 461. Vinogradova, O. I. *Colloids Surf. A: Physicochem. Eng. Aspects* **1994**, *82*, 247.
(20) Sykes, C.; Andrieu, C.; Détappe, V.; Deniau, S. *J. Phys. III Fr.* **1994**, *4*, 775. Brochard Wyart, F.; Daillant, J. *Can. J. Phys.* **1990**, *68*, 1084.
(21) Ohara, P. C.; Heath, J. R.; Gelbart, W. M. *Angew. Chem., Int. Ed. Engl.* **1997**, *36* (10), 1078.